Japanese Journal of Applied Physics **56**, 122501 (2017)
https://doi.org/10.7567/JJAP.56.122501

REGULAR PAPER

Paraxial ray solution for liquid-filled variable focus lenses

Lihui Wang[1]*, Hiromasa Oku[2], and Masatoshi Ishikawa[1,3]

[1]*Department of Creative Informatics, Graduate School of Information Science and Technology, The University of Tokyo, Bunkyo, Tokyo 113-8656, Japan*
[2]*Department of Electronics and Informatics, School of Science and Technology, Gunma University, Kiryu, Gunma 376-8515, Japan*
[3]*Department of Information Physics and Computing, Graduate School of Information Science and Technology, The University of Tokyo, Bunkyo, Tokyo 113-8656, Japan*

*E-mail: wang_lihui@ipc.i.u-tokyo.ac.jp

Received August 18, 2017; accepted October 12, 2017; published online November 21, 2017

We propose a general solution for determining the cardinal points and effective focal length of a liquid-filled variable focus lens to aid in understanding the dynamic behavior of the lens when the focal length is changed. A prototype of a variable focus lens was fabricated and used to validate the solution. A simplified solution was also presented that can be used to quickly and conveniently calculate the performance of the lens. We expect that the proposed solutions will improve the design of optical systems that contain variable focus lenses, such as machine vision systems with zoom and focus functions. © 2017 The Japan Society of Applied Physics

1. Introduction

Lenses are essential components in many optical systems, and are commonly used to transmit and/or bend light beams. Traditional lenses are constructed of solid materials, such as glass and plastic. In order to realize zoom or focus functions, the conventional approach is to employ two or more lenses, which are mechanically moved over specific distances. In recent years, compact optical systems using variable focus lenses have become popular, which is a term given to a single lens whose focal length can be changed dynamically.

Decades of research have been conducted into variable focus lenses, and numerous prototypes have been demonstrated. The focal length of a lens is defined by the curvature of the refractive surface and the media on both sides, and a variable focus lens can be realized if at least one of these factors can be controlled.[1,2] A liquid crystal (LC) lens forms a graded refractive index distribution by changing the orientations of the directors under an inhomogeneous electric field, thereby controlling the focal length.[3–5] Another approach is to manipulate the physical deformation of the refractive surface of a liquid-filled variable focus lens. In general, variable focus lenses can be classified as liquid–membrane (LM),[6–11] liquid–liquid (LL),[12–16] and liquid–membrane–liquid (LML) lenses.[17,18] Various driving approaches are available, such as fluidic pressure,[6–8,16–21] electrochemistry,[22] dielectric elastomer,[23–25] thermal effects,[26,27] environmentally adaptive hydrogel,[28] electro-wetting phenomenon,[12,13,29] and the dielectrophoresis phenomenon.[30,31]

Normally, when implementing an advanced optical system design, the thickness of the lens should be taken into account. However, due to the tunable optical performance of a variable focus lens, the cardinal points will dynamically change. To address this, we propose a paraxial general solution to determine the cardinal points and effective focal length based on a general model of a liquid-filled variable focus lens. This solution is flexible and can be applied to any type of liquid-filled variable focus lens, including LM, LL, and LML lenses.

2. Mathematical model of a liquid-filled variable focus lens

2.1 General model of a liquid-filled variable focus lens

Figure 1 shows a sketch of a variable focus lens with an LML structure, which includes two glass windows, two liquid media, and an elastic membrane. Ideally, the two types of liquid media should have a high transmittance and the same density so that the deflection profile of the elastic membrane will maintain a symmetric deformation, even when the lens is placed vertically. In this configuration, there will be a contrast of refractive indices between the two liquids, which allows the deflected surface to perform the function of a lens. The elastic membrane should have high transmittance and not react with the chosen liquids. When a uniform pressure is applied to the membrane, its surface will stretch and bulge accordingly, and this surface profile will serve as a refractive surface.

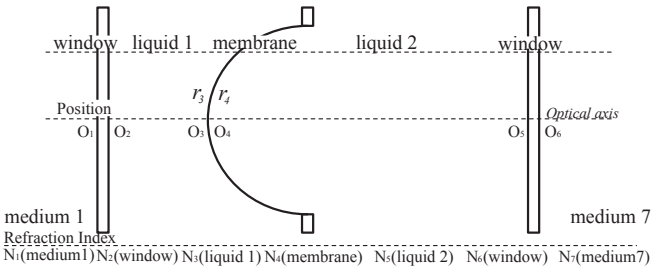

Fig. 1. Sketch of a variable focus lens with an LML structure, which includes two glass windows, two types of liquid media, and an elastic membrane. The profile of the elastic membrane is deformable and serves as a refractive surface.

In the figure, the refractive indices from left to right are as follows: N_1 is the refractive index of medium 1, N_2 is for the front glass window, N_3 is for the first liquid, N_4 is for the elastic membrane, N_5 is for the second liquid, N_6 is for the back glass window, and N_7 is for medium 2. The intersection points between each element and the optical axis are indicated as $O_1, O_2, \ldots, O_6$. The radii of curvature of the elastic membrane, r_3 and r_4, are variable values and, to simplify the calculation, the deformation is considered to be spherical. The radius of curvature of the other surfaces are infinite. Therefore, the distances O_2O_3 and O_4O_5 change depending on the change in the radius of the membrane.

The proposed lens system model is general, and therefore is applicable to other liquid-filled variable lenses. A typical LM lens is described in Ref. 10, where the chamber is filled with a single liquid and sealed with an elastic membrane. When additional liquid is pumped in, the resulting pressure will reshape the soft membrane and cause the focal length to

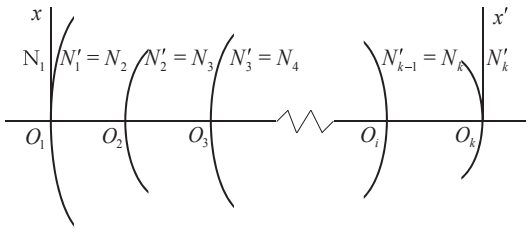

Fig. 2. Combination of the multiple optical systems used for the ray transfer matrix analysis.

change. In this general model, when air replaces one of the two liquids, the device model in Fig. 1 can be considered to represent an LM lens. Assume that the elastic membrane is removed and two immiscible liquids fill the two chambers but are connected with a circular hole.[15,16] In this case, the aperture size should be designed to be somewhat smaller than the capillary length,[18] which is the characteristic length scale for a liquid subjected to gravity and surface tension, so that gravity will be negligible. If these changes are made, the device model now describes an LL lens. Hence, we adopt the model in Fig. 1 as the starting point of our analysis.

2.2 Ray transfer matrix analysis

There are six optical surfaces in this system. We can abstract the general liquid lens model into multiple optical systems, as shown in Fig. 2. Here, a ray transfer matrix (RTM) analysis (i.e., the Schleiermacher equation) is employed to describe this optical system. This RTM analysis that is described below uses the paraxial approximation of ray optics, which means that all rays are assumed to be at a small angle and a small distance relative to the optical axis of the system.[32] There are i RTMs, where i ranges from 1 to 6.

All of the elements shown in Fig. 2 will be considered to be a single lens system. Elements 1, 2, 5, and 6, are assumed to be glass cover windows, and their refraction surfaces are considered to be plano surfaces. Hence, the RTMs of elements P_1, P_2, P_5, and P_6 will be simplified and are given by

$$P_1 = P_2 = P_5 = P_6 = \begin{pmatrix} 1 & 0 \\ 0 & 1 \end{pmatrix}. \tag{1}$$

Optical elements 3 and 4 are the tunable surfaces of the variable focus system, so their radii of curvature are variable parameters. The RTMs of elements P_3 and P_4 are given by

$$P_3 = \begin{pmatrix} 1 & 0 \\ \mu_3 & 1 \end{pmatrix}, \tag{2}$$

in which,

$$\mu_3 = \frac{N_4 - N_3}{r_3}, \tag{3}$$

$$P_4 = \begin{pmatrix} 1 & 0 \\ \mu_4 & 1 \end{pmatrix}, \tag{4}$$

in which,

$$\mu_4 = \frac{N_5 - N_4}{r_4}. \tag{5}$$

A transition matrix Δ_i describes transfer of the RTM matrix from the coordinate system in plane i to another coordinate system in plane $i + 1$,

$$\Delta_i = \begin{pmatrix} 1 & -\dfrac{\overline{O_iO_{i+1}}}{N_i + 1} \\ 0 & 1 \end{pmatrix}, \tag{6}$$

in which $\overline{O_iO_{i+1}}$ refers to the distance between O_i and O_{i+1}.

Hence, the complete RTM equation can be obtained by multiplying the above matrixes from plane 1 to plane 6.

The ray tracing matrix analysis is based on two reference planes, namely, the object and image planes, which are perpendicular to the optical axis of the system. The optical ray vectors in these planes are given by plane 1 $(X_1\ N_1u_1)^{\mathrm{T}}$ and plane 6 $(X'_6\ N_7u'_6)^{\mathrm{T}}$, in which the coordinate system was defined such that a light ray strikes the optical axis at a distance x, and the ray crosses the image plane at a distance x'. Here, u_i is the cosine of the optical direction x_i, and the elements marked with an apostrophe refer to the value at the back side of the original surface, such as $x_{i+1} = x'_i$.

The last surface of the system is plane 6. The total RTM of the variable focus lens system from plane 1 to plane 6 can be written as

$$\begin{pmatrix} X'_6 \\ N_7u'_6 \end{pmatrix} = P_6\Delta_5P_5\Delta_4P_4\Delta_3P_3\Delta_2P_2\Delta_1P_1\begin{pmatrix} X_1 \\ N_1u_1 \end{pmatrix}. \tag{7}$$

If the total transformation matrix is defined as $\widetilde{P}$, this equation can be rewritten as follows:

$$\begin{pmatrix} X'_6 \\ N_7u'_6 \end{pmatrix} = \widetilde{P}\begin{pmatrix} X_1 \\ N_1u_1 \end{pmatrix}, \tag{8}$$

where $\widetilde{P}$ is

$$\widetilde{P} = P_6\Delta_5P_5\Delta_4P_4\Delta_3P_3\Delta_2P_2\Delta_1P_1 = \begin{pmatrix} \widetilde{\chi} & \widetilde{\lambda} \\ \widetilde{\mu} & \widetilde{\upsilon} \end{pmatrix}. \tag{9}$$

The four elements of $\widetilde{P}$ are expressed by $\widetilde{\chi}$, $\widetilde{\lambda}$, $\widetilde{\mu}$, and $\widetilde{\upsilon}$, and the substitute equations are as follows:

$$\widetilde{\chi} = 1 + \left(-\frac{\overline{O_3O_4}}{N_4}\right) \times \frac{N_4 - N_3}{r_3} + \left(-\frac{\overline{O_4O_5}}{N_5} - \frac{\overline{O_5O_6}}{N_6}\right) \times \left\{\frac{N_5 - N_4}{r_4} + \left[\left(\frac{N_5 - N_4}{r_4}\right) \times \left(-\frac{\overline{O_3O_4}}{N_4}\right) + 1\right] \times \frac{N_4 - N_3}{r_3}\right\}, \tag{10}$$

$$\widetilde{\lambda} = \left\{1 + \left(-\frac{\overline{O_3O_4}}{N_4}\right) \times \frac{N_4 - N_3}{r_3} + \left(-\frac{\overline{O_4O_5}}{N_5} - \frac{\overline{O_5O_6}}{N_6}\right) \times \left\{\left[\left(\frac{N_5 - N_4}{r_4}\right) \times \left(-\frac{\overline{O_3O_4}}{N_4}\right) + 1\right] \times \frac{N_4 - N_3}{r_3} + \frac{N_5 - N_4}{r_4}\right\}\right\}$$
$$\times \left(-\frac{\overline{O_1O_2}}{N_2} - \frac{\overline{O_2O_3}}{N_3}\right) + \left\{\left(-\frac{\overline{O_3O_4}}{N_4}\right) + \left(-\frac{\overline{O_4O_5}}{N_5} - \frac{\overline{O_5O_6}}{N_6}\right) \times \left[\left(\frac{N_5 - N_4}{r_4}\right) \times \left(-\frac{\overline{O_3O_4}}{N_4}\right) + 1\right]\right\}, \tag{11}$$

$$\widetilde{\mu} = \frac{N_5 - N_4}{r_4} + \left[\left(\frac{N_5 - N_4}{r_4}\right) \times \left(-\frac{\overline{O_3O_4}}{N_4}\right) + 1\right] \times \frac{N_4 - N_3}{r_3}, \tag{12}$$

$$\widetilde{\upsilon} = \left\{\frac{N_5 - N_4}{r_4} + \left[\left(\frac{N_5 - N_4}{r_4}\right) \times \left(-\frac{\overline{O_3O_4}}{N_4}\right) + 1\right] \times \frac{N_4 - N_3}{r_3}\right\} \times \left(-\frac{\overline{O_1O_2}}{N_2} - \frac{\overline{O_2O_3}}{N_3}\right) + \left[\left(\frac{N_5 - N_4}{r_4}\right) \times \left(-\frac{\overline{O_3O_4}}{N_4}\right) + 1\right]. \tag{13}$$

3. Cardinal points of a variable focus lens and the effective focal length

In Fig. 3, reference plane F is at a distance z from the first plane of the lens, and another reference plane F' is at a distance z' from the last plane of the lens. In the figure, $z < 0$ and $z' > 0$. The transformation matrix Δ_0 from plane F to plane O is

$$\Delta_0 = \begin{pmatrix} 1 & -\frac{-z}{N_1} \\ 0 & 1 \end{pmatrix}, \tag{14}$$

and the transformation matrix Δ_6 from plane O' to plane F' is

$$\Delta_6 = \begin{pmatrix} 1 & -\frac{z'}{N_7} \\ 0 & 1 \end{pmatrix}. \tag{15}$$

The RTM from the object plane to the image plane is written as

$$P = \begin{pmatrix} \chi & \lambda \\ \mu & \upsilon \end{pmatrix} = \begin{pmatrix} 1 & -\frac{z'}{N_7} \\ 0 & 1 \end{pmatrix} \widetilde{P} \begin{pmatrix} 1 & -\frac{-z}{N_1} \\ 0 & 1 \end{pmatrix}. \tag{16}$$

Substituting $\widetilde{P}$ with $\widetilde{\chi}$, $\widetilde{\lambda}$, $\widetilde{\mu}$, and $\widetilde{\upsilon}$, the RTM equation can be rewritten as

$$\begin{aligned} P &= \begin{pmatrix} 1 & -\frac{-z'}{N_7} \\ 0 & 1 \end{pmatrix} \begin{pmatrix} \widetilde{\chi} & \widetilde{\lambda} \\ \widetilde{\mu} & \widetilde{\upsilon} \end{pmatrix} \begin{pmatrix} 1 & -\frac{-z}{N_1} \\ 0 & 1 \end{pmatrix} \\ &= \begin{pmatrix} \widetilde{\chi} - \widetilde{\mu}\frac{z'}{N_7} & \widetilde{\lambda} - \widetilde{\upsilon}\frac{z'}{N_7} + \frac{z}{N_1}\left(\widetilde{\chi} - \widetilde{\mu}\frac{z'}{N_7}\right) \\ \widetilde{\mu} & \widetilde{\upsilon} + \widetilde{\mu}\frac{z}{N_7} \end{pmatrix}. \end{aligned} \tag{17}$$

Since F and F' are the front and rear focal points, respectively, it is necessary that $\widetilde{\lambda} = 0$. The reason for this can be found in the following equation:

$$\begin{pmatrix} x' \\ N'u' \end{pmatrix} = \begin{pmatrix} \widetilde{\chi} & \widetilde{\lambda} \\ \widetilde{\mu} & \widetilde{\upsilon} \end{pmatrix} \begin{pmatrix} x \\ Nu \end{pmatrix}, \tag{18}$$

in which substituting $\lambda = 0$ yields

$$x' = \widetilde{\chi} x. \tag{19}$$

This means that light coming from point F will be focused at point F' regardless of the angle of the light. In the following sections, this condition is used to calculate the cardinal points.

3.1 Front and back focal length

When light converges at point F', parallel light will be focused at a single point, and $\widetilde{\chi} = 0$. The distance from the last surface of a lens to its image plane is defined as the back focal length (BFL), and can be written as

$$\mathrm{BFL} = z'(\mathrm{BFL}) = N_7 \frac{\widetilde{\chi}}{\widetilde{\mu}}. \tag{20}$$

Similarly, if light is conjugate at point F, then $\widetilde{\upsilon} = 0$, and parallel light will be focused at a single point. The following condition for the front focal point will be satisfied for the front focal length (FFL), which is given by

$$\mathrm{FFL} = z(\mathrm{FFL}) = -N_1 \frac{\widetilde{\upsilon}}{\widetilde{\mu}}. \tag{21}$$

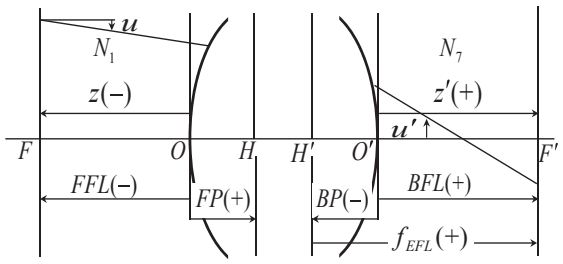

Fig. 3. Illustration of the characteristic points of a lens system, which was used when analyze the cardinal points and effective focal length.

3.2 Principal points

The principal points are the conjugate points that provide the lateral magnification of +1. If F and F' are conjugate points, $\widetilde{\lambda} = 0$ must hold. Thus, $x' = \widetilde{\chi}x$, and the lateral magnification is $\frac{x'}{\chi} = x$. Here, $\widetilde{\lambda} = 0$ and $\widetilde{\chi} = 1$; thus, $\widetilde{\chi}\widetilde{\upsilon} - \widetilde{\lambda}\widetilde{\mu} = 1$. The front principal point (FP) is defined as follows:

$$\mathrm{FP} = z(\mathrm{FP}) = -N_1 \frac{1}{\widetilde{\mu}}(\widetilde{\upsilon} - 1). \tag{22}$$

Similarly, the back principal point (BP) is defined as

$$\mathrm{BP} = z'(\mathrm{BP}) = N_7 \frac{1}{\widetilde{\mu}}(\widetilde{\chi} - 1). \tag{23}$$

3.3 Effective focal length

The effective focal length (f_{EFL}) is the distance between the back principal point and the back focal length. The f_{EFL} is not related to the cardinal points, but is an important parameter in optics design. According to the diagram of the characteristic points shown in Fig. 3, when the BFL and BP are known, the f_{EFL} of the system can be written as

$$f_{\mathrm{EFL}} = \mathrm{BFL} + (-\mathrm{BP}) = N_7 \frac{\widetilde{\chi}}{\widetilde{\mu}} + \left[-N_7 \frac{1}{\widetilde{\mu}}(\widetilde{\chi} - 1)\right] = N_7 \frac{1}{\widetilde{\mu}}. \tag{24}$$

4. Discussion and experiment

4.1 Configuration of the interface profile

In Fig. 1, the elastomer membrane acts as a wall separating the two chambers, effectively creating a circular boundary condition. The deformation happens at the interface between the two liquids, and acts as a refractive surface due to the difference in the refractive indices of the two liquids. If one liquid was made to flow into and out of its chamber while the other remained sealed, the lens could dynamically change its focal length. The geometrical surface is important to the lens system, and will be discussed in this subsection.

The curved surface of the membrane is assumed to be symmetric and uniform, the surface tension T per unit length

along the boundary is constant, and the lens has a fixed aperture $2a$. Pressure P is uniformly applied to the membrane. If the deflection of the membrane satisfies the circular boundary conditions, the deflection Z has the following relationship with the radius r:

$$Z(r) = \frac{P}{4T}(a^2 - r^2). \tag{25}$$

Equation (25) illustrates that the bulged membrane presents a parabolic profile. However, the lens may sometimes be placed in a vertical direction, and consequently, the lens profile will not be symmetrical due to the effect of gravity on the liquid(s). If a better liquid-pair can be employed, the LL and LML lenses may perform better than an LM lens.[33] However, it is difficult to prepare liquids to have the same density at any temperature due to the influence of thermal expansion.[34]

The effects of gravity will deform the shape of a liquid-filled lens in practice. When the lens is placed vertically for normal use, the effect of gravity on the lens shape is at a maximum, as shown in Fig. 4. In some cases, the gravitational force distorting the shape of the membrane may be negligible, even when the lens is placed in a vertical direction. According to Sugiura's derivation,[9] the shape of the elastic membrane can be described by the following:

$$Z = -\frac{\rho g a}{T}\left[\left(y^2 - \frac{y^3}{6a} - \frac{4}{3}ay\right) + k(y^2 - 2ay)\right], \tag{26}$$

where ρ is the density of the liquid, g is the gravitational constant (9.8 m/s^2), and k is a parameter related to P, ρ, and a as

$$k = -\frac{P}{2\rho g a}. \tag{27}$$

According to Eq. (26), the profile of the elastic membrane is a parabolic-like shape.

When the membrane is not significantly deformed in comparison with its aperture, this surface can be approximated by a spherical shape. With such an approximation, the resulting error will be very small. Therefore, a standard spherical lens profile can be employed to accommodate the liquid lens. According to Fig. 5, the parabolic and spherical shapes shown have a common base aperture and the same maximum displacement h. According to Knollamn's analysis,[11] the maximum error in the displacement is

$$\Delta_{Z_{MAX}} < h\left(\frac{h}{2a}\right)^2. \tag{28}$$

If the altitude of the lens satisfies

$$h \ll 2a, \tag{29}$$

with respect to the lens aperture, then the error will be negligible. The value of the maximum error in the displacement is quite small, and is within the tolerance of the surface roughness of a conventional spherical glass lens. Therefore, we consider the proposed model of the liquid-filled lens to be a standard spherical lens.

4.2 Experiment result

We compared the results of the above equations with the experimental results obtained from a prototype of an LML variable focus lens model. A CAD drawing of an exploded view of the LML variable focus lens model is shown in the upper part of Fig. 6, and a photo of the prototype lens is shown in the lower part. Inserts 1 and 2 show the two liquid chambers. The circular hole was stiff so as to hold the membrane and ensure the circular boundary condition was maintained while the membrane was being deformed. The thickness of each layer is as follows: ~0.5 mm for glass windows 1 and 2, ~2.0 mm for inserts 1 and 2, ~0.5 mm for the circular hole, and ~0.07 mm for the membrane. The reflective indices of the LML lens media are shown in Table I. The refractive surface $\overline{O_3O_4}$ was bent toward the front and back with two different curvatures, r_f and r_b, because the aperture size of this prototype presented two values when bent in different directions, $D_f = 31$ mm and $D_b = 30$ mm.

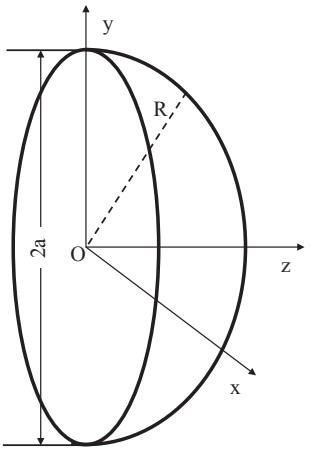

Fig. 4. Shape profile of a liquid-filled variable focus lens placed vertically.

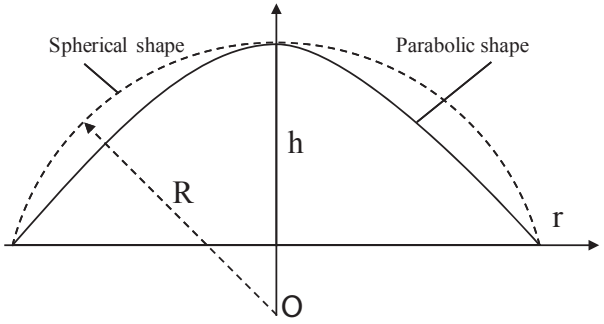

Fig. 5. Approximation of a parabolic liquid lens profile with a spherical shape. The parabolic and spherical shapes have the same base aperture $2a$ and the same maximum displacement h.

When the membrane was deflected toward window 2, the maximum deflection height was $h = 2$ mm. In this case, the distances were $\overline{O_2O_3} = 4.5$ mm and $\overline{O_4O_5} = 0$ mm. The curvature of the membrane can be calculated from $r_f^2 = (D_f/2)^2 + (r_f - 2)^2$, and an $r_f = -61.0625$ mm was adopted due to the direction of deflection. Then, values for the four elements $\widetilde{\chi}$, $\widetilde{\lambda}$, $\widetilde{\mu}$, and $\widetilde{\upsilon}$ of $\widetilde{P}$ were calculated as

$$\widetilde{P}_f = \begin{pmatrix} \widetilde{\chi} & \widetilde{\lambda} \\ \widetilde{\mu} & \widetilde{\upsilon} \end{pmatrix} = \begin{pmatrix} 0.9995 & -3.8761 \\ 0.0014 & 0.9950 \end{pmatrix}. \tag{30}$$

The back focal length was calculated according to Eq. (20), and $BFL_f = 701.5588$ mm. The back principal point was $BP_f = -0.3179$ mm, according to Eq. (23). Meanwhile, according to Eq. (24), the effective focal length was $f_{EFL_f} = BFL_f + (-BP_f) = 701.8767$ mm.

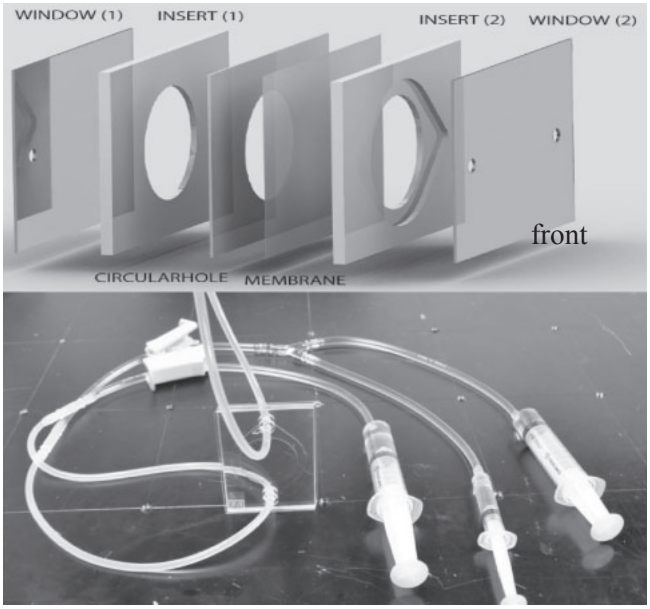

Fig. 6. (Upper) Exploded view of the LML variable focus lens model. (Lower) Photo of a prototype lens with its driving mechanism. Two chambers were infused with ultra-pure water and 50% sucrose water. One liquid was made to flow freely, while the end of the tube of the other chamber was blocked. The power of the lens could be shifted dynamically from positive to negative by pushing or pulling the syringe.

Table I. Parameters of the LML lens.

Media	Refractive index
Air	$N_1 = 1.000$
Glass window	$N_2 = 1.518$
Sucrose water (50%)	$N_3 = 1.420$
PDMS polymer	$N_4 = 1.400$
Ultra-pure water	$N_5 = 1.333$
Glass window	$N_6 = 1.518$
Air	$N_7 = 1.000$

When the membrane was deflected toward window 1, the maximum deflection height was $h = 2.5\,\text{mm}$. The distances were $\overline{O_2O_3} = 0\,\text{mm}$ and $\overline{O_4O_5} = 4.5\,\text{mm}$. The curvature of the membrane can be calculated from $r_b^2 = (D_b/2)^2 + (r_b - 2.5)^2$ and $r_b = 46.25\,\text{mm}$. The four elements $\widetilde{\chi}$, $\widetilde{\lambda}$, $\widetilde{\mu}$, and $\widetilde{\upsilon}$ of $\widetilde{P}$ were:

$$\widetilde{P}_b = \begin{pmatrix} \widetilde{\chi} & \widetilde{\lambda} \\ \widetilde{\mu} & \widetilde{\upsilon} \end{pmatrix} = \begin{pmatrix} 1.0006 & -3.8800 \\ -0.0019 & 1.0067 \end{pmatrix}. \quad (31)$$

Similarly, the back focal length was $\text{BFL}_b = -531.9182\,\text{mm}$, the back principal point was $\text{BP}_b = -0.3179\,\text{mm}$, and the effective focal length was $f_{\text{EFL}_b} = \text{BFL}_b + (-\text{BP}_b) = -531.6003\,\text{mm}$.

The dynamic tunable range of the optical power, which is equal to the reciprocal of the focal length with units of inverse meters, can be described as

$$\widetilde{\phi}_{\text{power}} = \frac{1}{f_{\text{EFL}}} = -\frac{10^3}{531.6003} \sim \frac{10^3}{701.8767}\,(\text{m}^{-1}). \quad (32)$$

The tunable focal length range of the LML prototype was measured. Because the focal length of the LML lens was designed to change its focal length from −531.6003 to +701.8767, a solid glass lens (focal length $f_1 = 210\,\text{mm}$) was placed before the LML liquid lens at a certain distance ($D = 100\,\text{mm}$) so that the combined focal length became positive and measurable. As shown in Fig. 7, when a parallel beam shone from the left of the glass lens ($f_1 = S_1$) and passed through the liquid lens (test lens, f_2), the focus point (S_2) could be found. The focal length of the test lens f_2 can be deduced from

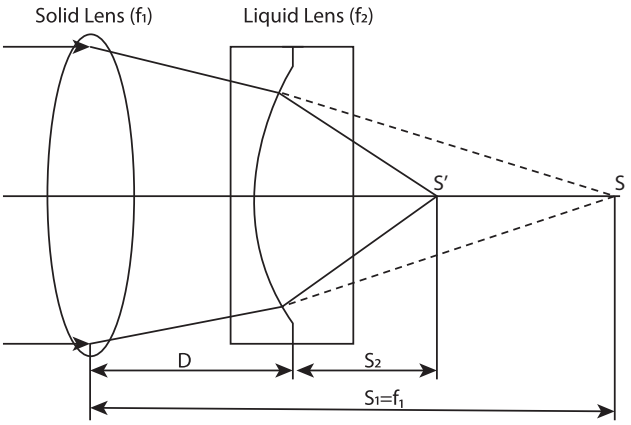

Fig. 7. Experimental setup to measure the tunable focal range of the LML lens. Because the focal length of the LML lens was designed to change from negative to positive, a positive glass lens was placed before the test lens so that the combined focal length became positive and measurable.

$$\frac{1}{f_2} = \frac{1}{S_2} - \frac{1}{S_1 - D}. \quad (33)$$

In our experiment, ultra-pure water (purified by DirectQ-UV Millipore, refractive index of 1.333) was used as one liquid, and the other was 50% sucrose water (sucrose mixed with ultra-pure water, the overall refractive index was 1.4216). A poly(dimethylsiloxane) (PDMS) elastic membrane (refractive index of 1.40) with a 0.07 mm thickness was inserted and used to separate the two liquids. Liquids have slow diffusion and convection compared to solids. So, the properties of liquids can be sensitive to temperature variation, which will result in fluctuation of the lens properties. Hence, the experiment was conducted under a constant room temperature of 25 °C. An observer plate was placed on the other side of the liquid lens to observe the smallest focal spot and fixed in position. Then, the distance between the observer plate and the liquid lens S_2 was recorded to calculate the focal length of the liquid lens according to Eq. (33). When the LML lens was operated with a positive power, S_2 was measured as 110 mm and the maximum focal length was 696.67 mm. Meanwhile, when the lens was operated at a negative power, S_2 was measured as 135 mm and the minimum focal length was −594.00 mm.

The process of preparing the sucrose water was not exact; consequently, there was a small difference between the ideal refractive index and the actual one. In order to increase the refractive index of the sucrose water, the density of the sucrose water was greater than that of the pure water side, which resulted in an asymmetric deflection on the surface profile, and may have affected the measurement of the focal length. Nevertheless, the experiment results agree with the theoretical tunable focal length range, which was calculated using Eq. (32).

4.3 Feasibility and simplification

The general solution was deduced from the general model of an LML lens; however, the solution can also be used on LM and LL lenses. The procedure for determining the characteristics of an LM lens is similar to that for an LML lens. If one of the liquids is replaced by air, which means one of the refractive indices of the two liquids is equal to 1 ($N_3 = 1$ or $N_5 = 1$), the lens system can be considered to be an LM lens. These values are then inserted into the relevant equations, and the results are computed. When the elastic membrane is removed, and two immiscible liquids fill the two chambers, the lens model is then representative of an LL lens. In this case, $\overline{O_3O_4} = 0$, $N_4 = 0$, and $\overline{O_3O_4}/N_4 = 0$. The two immiscible liquids are connected via a circular hole, which means they have a connecting interface; hence, the bending radii of the interface are equal, i.e., $r_3 = r_4$. This is a precondition for solving the equations for an LL lens.

It is possible to simplify the calculation if the thickness of the elastic membrane is negligible. This specific condition is similar to that for the LL lens model, where the characteristics of the membrane are $\overline{O_3O_4} = 0$, $N_4 = 0$, $\overline{O_3O_4}/N_4 = 0$, and the bending radii of the interface are equal, i.e., $r_3 = r_4 = r$. Meanwhile, medium 1 and medium 7 can be considered to be air under normal conditions, which means $N_1 = N_7 = 1$.

According to the general solution, when calculating the effective focal length, $\widetilde{\mu}$ is used and $\widetilde{\chi}$ and $\widetilde{v}$ are employed to compute the cardinal points. Hence, $\widetilde{\lambda}$ is not included in the transfer matrix $\widetilde{P}$. If $\widetilde{\mu}$ is defined by $\widetilde{\mu} = (N_5 - N_3)/r$, then $\widetilde{P}$ can be rewritten as follows:

$$\widetilde{P} = \begin{pmatrix} 1 - \widetilde{\mu}\left(\dfrac{\overline{O_4O_5}}{N_5} + \dfrac{\overline{O_5O_6}}{N_6}\right) & \widetilde{\lambda} \\ \widetilde{\mu} & 1 - \widetilde{\mu}\left(\dfrac{\overline{O_1O_2}}{N_2} + \dfrac{\overline{O_2O_3}}{N_3}\right) \end{pmatrix}. \tag{34}$$

Thus, the BFL, FFL, BP, and FP can be modified in the following equations:

$$\mathrm{BFL} = \frac{1}{\widetilde{\mu}} - \left(\frac{\overline{O_4O_5}}{N_5} + \frac{\overline{O_5O_6}}{N_6}\right). \tag{35}$$

$$\mathrm{FFL} = -\frac{1}{\widetilde{\mu}} + \left(\frac{\overline{O_1O_2}}{N_2} + \frac{\overline{O_2O_3}}{N_3}\right). \tag{36}$$

$$\mathrm{BP} = -\frac{\overline{O_4O_5}}{N_5} - \frac{\overline{O_5O_6}}{N_6}. \tag{37}$$

$$\mathrm{FP} = \frac{\overline{O_1O_2}}{N_2} + \frac{\overline{O_2O_3}}{N_3}. \tag{38}$$

The BP is defined by the characteristics of the back glass windows (thickness $\sim\overline{O_5O_6}$ and refractive index $\sim N_6$), and the characteristics of the liquid medium (thickness $\sim\overline{O_4O_5}$ and refractive index $\sim N_5$). For these four parameters, $\overline{O_4O_5}$ changes as the bending curvature of the surface changes. The FP has a similar relationship to the characteristics of the front glass windows and the liquid medium on the other side. The BFL and FFL can be computed based on the value of the BP and FP by separately adding and subtracting the value of $1/\widetilde{\mu}$. A simplified method of computing the effective focal length is given in the following equation:

$$f_{\mathrm{EFL}} = \frac{1}{\widetilde{\mu}} = \frac{r}{N_5 - N_3}. \tag{39}$$

Note that the above simplification is based on the assumptions that the thickness of the elastic membrane is negligible and the lens system is in air. The assumption that the lens in air is valid most of the time and, in cases where the thickness of the membrane is small enough, the simplified form of the equation will be convenient. For example, if we computed the effective focal length of the prototype lens in Sect. 4.2 using Eq. (39), the result would have been (−531.6092 to 701.8678) mm. The error between this result and that for Eq. (32) is only −0.0089 mm. This level of error is acceptable, given that the membrane in the prototype lens was 0.07 mm thick. In summary, Eqs. (20)–(24) provide an accurate solution, while the simplifications in Eqs. (35)–(39) provide a convenient methodology when applicable.

5. Conclusions

Lenses are a fundamental component in photonics, and the corresponding cardinal points and effective focal length are widely used to evaluate lens performance in optical systems. Because the dynamic optical performance of a variable focus lens is complex, a general solution is desirable to enable designers to better understand the behavior of this type of lens. In the work described in this paper, we studied a general liquid-filled variable lens model and proposed a paraxial general solution for computing the cardinal points, principal points, front and back focal lengths, and effective focal length. The proposed general equations are flexible and can be applied to any type of liquid-filled variable focus lens, including LM, LL, and LML lenses. A prototype of an LML variable focus lens was fabricated, and good agreement was found between the experimental results of its dynamic focal length range and those of the proposed general solution. A simplification of the general solution was then presented to facilitate quick and convenient calculation of lens performance. We anticipate that this general solution will provide a solid understanding of the dynamic performance of a variable focus lens, and will prove useful when designing optical systems. This solution can also be utilized to develop an implementation scheme when designing a focusing system employing a varifocal lens or a zooming system employing two or more varifocal lenses, so that the specific performance index of the varifocal lens(es) and the system performance, such as the scale of the system, tunable focal length range, and zoom factor, can be investigated. Furthermore, the solution can also help select appropriate liquids, elastomer, and other candidates to fabricate a specific varifocal lens with a target performance.

Acknowledgments

This work was supported by JSPS KAKENHI Grant-in-Aid for Young Scientists B 15K16035 and partially supported by Konica Minolta Inc.

1) H. Ren and S.-T. Wu, *Introduction to Adaptive Lenses* (Wiley, New York, 2012) Vol. 75.
2) J. E. Greivenkamp, *Field Guide to Geometrical Optics* (SPIE Press, Bellingham, WA, 2004) Vol. 1.
3) S. Sato, Jpn. J. Appl. Phys. **18**, 1679 (1979).
4) M. Ye, B. Wang, M. Uchida, S. Yanase, S. Takahashi, and S. Sato, Appl. Opt. **51**, 7630 (2012).
5) G. Li, D. L. Mathine, P. Valley, P. Äyräs, J. N. Haddock, M. Giridhar, G.

Williby, J. Schwiegerling, G. R. Meredith, B. Kippelen, S. Honkanen, and N. Peyghambarian, Proc. Natl. Acad. Sci. U.S.A. **103**, 6100 (2006).
6) H. Oku, K. Hashimoto, and M. Ishikawa, Opt. Express **12**, 2138 (2004).
7) H. Oku and M. Ishikawa, 16th Annu. Meet. IEEE Lasers and Electro-Optics Society (LEOS 2003), 2003, Vol. 1, p. 309.
8) S. Xu, H. Ren, Y.-J. Lin, M. J. Moharam, S.-T. Wu, and N. Tabiryan, Opt. Express **17**, 17590 (2009).
9) N. Sugiura and S. Morita, Appl. Opt. **32**, 4181 (1993).
10) H. Ren, D. Fox, P. A. Anderson, B. Wu, and S.-T. Wu, Opt. Express **14**, 8031 (2006).
11) G. Knollman, J. Bellin, and J. Weaver, J. Acoust. Soc. Am. **49**, 253 (1971).
12) B. Berge and J. Peseux, Eur. Phys. J. E **3**, 159 (2000).
13) S. Kuiper and B. Hendriks, Appl. Phys. Lett. **85**, 1128 (2004).
14) C.-C. Cheng, C. A. Chang, and J. A. Yeh, Opt. Express **14**, 4101 (2006).
15) S. Xu, Y. Liu, H. Ren, and S.-T. Wu, Opt. Express **18**, 12430 (2010).
16) H. Oku and M. Ishikawa, Appl. Phys. Lett. **94**, 221108 (2009).
17) L. Wang, H. Oku, and M. Ishikawa, Appl. Phys. Lett. **102**, 131111 (2013).
18) L. Wang, H. Oku, and M. Ishikawa, Opt. Express **22**, 19448 (2014).
19) A. Mondol, B. Vogel, and G. Bastian, Opt. Express **23**, A692 (2015).
20) N. Hasan, A. Banerjee, H. Kim, and C. H. Mastrangelo, Opt. Express **25**, 1221 (2017).
21) F. Santiago, B. Bagwell, T. Martinez, S. Restaino, and S. Krishna, J. Opt. Soc. Am. A **31**, 1842 (2014).
22) C. A. López, C.-C. Lee, and A. H. Hirsa, Appl. Phys. Lett. **87**, 134102 (2005).
23) B. Jin, J.-H. Lee, Z. Zhou, G. Zhang, G.-B. Lee, H. Ren, and C. Nah, Opt. Eng. **55**, 017107 (2016).
24) S. Shian, R. M. Diebold, and D. R. Clarke, Opt. Express **21**, 8669 (2013).
25) L. Maffli, S. Rosset, M. Ghilardi, F. Carpi, and H. Shea, Adv. Funct. Mater. **25**, 1656 (2015).
26) L. Miccio, A. Finizio, S. Grilli, V. Vespini, M. Paturzo, S. De Nicola, and P. Ferraro, Opt. Express **17**, 2487 (2009).
27) A. O. Ashtiani and H. Jiang, Appl. Phys. Lett. **103**, 111101 (2013).
28) L. Dong, A. K. Agarwal, D. J. Beebe, and H. Jiang, Nature **442**, 551 (2006).
29) F. Mugele and J.-C. Baret, J. Phys.: Condens. Matter **17**, R705 (2005).
30) H. Ren, S. Xu, and S.-T. Wu, Lab Chip **13**, 100 (2013).
31) S. Xu, H. Ren, and S.-T. Wu, J. Phys. D **46**, 483001 (2013).
32) A. Nussbaum, Proc. SPIE **3190**, 34 (1997).
33) F. Schneider, J. Draheim, R. Kamberger, P. Waibel, and U. Wallrabe, Opt. Express **17**, 11813 (2009).
34) H. Zhang, H. Ren, S. Xu, and S.-T. Wu, Opt. Express **22**, 1930 (2014).